Multiequipment Radiation Measurements in a Field Generated by Bombarding a 1-GeV/u Fe Beam on a Polyethylene Target at GSI and Comparison to FLUKA Simulations

Sarath Kundumattathil Mohanan, Hamza Boukabache, *Member, IEEE*, Robert Froeschl, Felix Horst, Ekaterina Kozlova, Tommaso Lorenzon, Daniel Perrin, and Alexey Sokolov

***Abstract*— The complex nature of the radiation environment in various high-energy physics facilities necessitates the use of different kinds of radiation monitors. The detectors used could be either passive or active and need dedicated read-out electronics. The present study was conducted at GSI Helmholtzzentrum für Schwerionenforschung in Cave A where different kinds of radiation detectors were tested in parallel in the secondary radiation field generated by a 1-GeV/u ^{56}Fe ion beam impinging a thick polyethylene target, and their responses were compared with the Monte Carlo code FLUKA simulations. Thermoluminescence-based passive detectors from GSI, ionization chamber-based radiation monitors developed by CERN, WENDI-II, and wide-range photon detectors from Berthold and Thermo Fisher were studied in this campaign. The study showed good agreement between the temporal responses of the various detectors, and comparison of the ambient dose equivalents measured with the simulations showed agreement of over 40% for all the detectors. In addition, two versions of radiation monitoring front-ends developed at CERN were directly compared and the relative mismatch in measurement was consistently less than 10%.**

***Index Terms*— Detectors benchmarking, FLUKA simulations, ionization chamber, neutron detector, radiation monitoring, Roentgen equivalent man (REM) counters.**

Manuscript received 19 October 2023; accepted 29 November 2023. Date of publication 4 December 2023; date of current version 15 February 2024. This work was supported in part by the European Space Agency (ESA)-Investigations into Biological Effects of Radiation (IBER) 19 Project; and in part by the Experiment IBER-010, which was Performed in Cave A at the GSI Helmholtzzentrum für Schwerionenforschung GmbH (GSI) Helmholtzzentrum fuer Schwerionenforschung, Darmstadt (Germany) in the Frame of Facility for Antiproton and Ion Research in Europe GmbH (FAIR) Phase-0. *(Corresponding author: Sarath Kundumattathil Mohanan.)*

Sarath Kundumattathil Mohanan, Hamza Boukabache, Robert Froeschl, Tommaso Lorenzon, and Daniel Perrin are with the CERN Radiation Protection, 1211 Geneva, Switzerland (e-mail: sarath.mohanan@cern.ch; hamza.boukabache@cern.ch; robert.froeschl@cern.ch; tommaso.lorenzon@cern.ch; daniel.perrin@cern.ch).

Felix Horst was with the Biophysics Department, GSI Helmholtzzentrum für Schwerionenforschung GmbH, 64291 Darmstadt, Germany. He is now with the OncoRay—National Center for Radiation Research in Oncology, University Hospital Carl Gustav Carus, Helmholtz-Zentrum Dresden-Rossendorf, Technische Universität Dresden, 01309 Dresden, Germany (e-mail: felix.horst@oncoray.de).

Ekaterina Kozlova and Alexey Sokolov are with the Radiation Protection and Safety Department, GSI Helmholtzzentrum für Schwerionenforschung GmbH, 64291 Darmstadt, Germany (e-mail: E.Kozlova@gsi.de; Al.Sokolov@gsi.de).

Color versions of one or more figures in this article are available at https://doi.org/10.1109/TNS.2023.3338820.

Digital Object Identifier 10.1109/TNS.2023.3338820

I. Introduction

RADIATION fields around high-energy particle accelerator facilities contain many different particles (neutrons, light charged particles, photons, etc.) which have a wide energy distribution. The properties of the radiation fields depend on different operation parameters such as the energy of the primary beam, the type of the projectile and the target, the geometry of the beam interaction points, and others. The situation becomes even more complex when the operating mode changes frequently, as is the case in most scientific facilities. Nevertheless, the dominant radiation outside the accelerator shielding barriers is the neutron field, with variable and usually minor contribution from other particles. An exception is the forward direction for high-intensity beams, for example, of protons with an energy greater than 10 GeV, where the radiation behind thick shielding is dominated by muons.

At a high-energy accelerator complex like GSI Helmholtzzentrum für Schwerionenforschung, the radiation fields have a broad energy range from thermal up to GeVs and the dose rates can reach up to several Sv/h. GSI operates SIS 18, a heavy-ion synchrotron, where any ion species from proton to uranium can be accelerated. In Cave A, situated downstream to the south from the synchrotron, ion beams, such as carbon ions, and very heavy ions, such as uranium, can be delivered in the energy range from 100 MeV to 1 GeV per nucleon. An experiment was carried out in Cave A within the ESA-IBER program [1], [2], [3] for space radiation shielding studies which produced a secondary radiation field by 1-GeV/u ^{56}Fe ions stopped in a thick polyethylene target. The aim of the study presented here was the characterization of the mixed field in and outside of Cave A, generated in this experiment, from the viewpoint of operational radiation protection using a variety of active detectors and passive dosimeters. The study compares the legacy radiation monitors, used typically in high-energy physics facilities, such as WENDI-II [4] neutron probe, gamma probes from Thermo Fisher [4] and Berthold [5], and thermoluminescent dosimeter (TLD)-based passive dosimeters with the new generation of radiation monitors developed at CERN. Though each of these monitors has already been extensively studied [6], [7], a comparative study

of all these devices in a neutron and light ion dominated field has never been carried out. The full detector setup was calibrated with two different sources ^{241}Am-Be(α, n) and ^{137}Cs. The experimental results were finally compared with the Monte Carlo simulations performed with the FLUKA code [8], [9], [10] version 4-3.2, hosted by CERN. It is the first time this FLUKA version is benchmarked in such a radiation field.

II. Radiation Detectors

Ionization chambers, proportional counters, scintillation detectors, Geiger counters, semiconductor detectors. and thermoluminescent dosimeters are the main types of radiation detectors used in dosimetry. This section details the different radiation detectors that were used in this measurement campaign.

A. Pressurized Ionization Chambers

The basic operational principle is based on the ionization of gas molecules caused by incident particles traversing the active medium. The choice of the gas depends on the application, the nature of particles, and their energies. The higher the gas pressure, the better the sensitivity of the detector.

In this experiment, to measure dose rates from radiation fields dominated by neutrons and mixed radiation fields, hydrogen-filled ionization chambers pressurized at 20 bars were used (IG5H20). The gas is confined into a steel made container of 5.2 L. The chambers used were manufactured by Centronic and are mainly operated for CROME system at CERN [11].

B. Air-Filled Ionization Chambers

Air-filled ionization chambers under atmospheric pressure are typically used for the measurement of residual dose rates. They are sensitive to mixed fields composed of neutrons, photons, protons, positrons, electrons, muons, pions, and kaons. They are typically installed at CERN [11] close to the accelerator and experiment components and are exposed to strong radiation fields during operation. They are made of graphite and plastic to minimize the activation of materials of the chamber itself [12]. The operational principle of this detector is similar to pressurized ionization chambers. For this experiment, air-filled ionization chambers manufactured by PTW were used (PMI T32006).

The technical aspects related to both kinds of ionization chambers used in this experiment are summarized in Table I.

TABLE I
Technical Data of Used Ionization Chambers

Detector	IG5H20	PMI
Dose rate range	50 nSv/h → 100mSv/h	500 nSv/h → 10 Sv/h
Photons energy range	65 keV → 10 MeV	10 keV → 1e5 MeV
Outer diameter	183 mm	158 mm
Length	4560 mm	215 mm
Detection	Mixed Field	Mixed Field
Gas	Hydrogen	Air

C. WENDI-II

The FHT-762 WENDI-II is a Roentgen equivalent man (REM) counter used to measure the ambient dose equivalent rate due to neutrons over a wide range of energy up to GeV levels. It uses a proportional counter tube filled with ^{3}He at a pressure of 2 bar inside a polyethylene moderator. The tube is surrounded with tungsten powder inside the moderator shell to increase the response above 10 MeV.

D. Thermoluminescent-Based Dosimeters

At GSI, thermoluminescent-based passive radiation monitors (TLD) are widely used. The sensitive elements in these detectors are thermoluminescent crystals. There are two types of detectors: GSI balls for the detection of neutrons and GSI cylinders to detect all other particles except neutrons. Both kinds of detectors are equipped with one card carrying four TLD crystals. In the GSI ball, for neutron detection, two of these crystals are of the TLD600H type, which mainly consists of ^{6}LiF and is sensitive to the low-energy neutrons and ionizing radiation in general. Two further crystals are of the TLD700H type, containing mainly ^{7}LiF and practically not sensitive to neutrons. The absorbed dose in TLD700H should be subtracted from the absorbed dose in TLD600H to obtain the neutron dose only. A polyethylene moderator with a radius of 16.5 cm surrounds the TLD elements for the detection of high-energy neutrons. To receive an isotropic response, a spherical form of the moderator was chosen. This device can be used to estimate the ambient dose equivalent $H^*(10)$ [13] for neutron energies from thermal up to about 10 MeV. To extend the response to neutrons of energies higher than 10 MeV, the moderator can be equipped with an additional layer of lead. This layer serves as a spallation target for high energetic neutrons and thus produces additional neutrons with lower energies which are suitable to increase the response of the dosimeter. In this case, the detection of neutrons of 20 MeV and higher is possible [14], [15]. For the GSI cylinder, a TLD card equipped only with TLD700H crystals is situated in the middle of a polyethylene cylinder with a radius of 2.5 and 6 cm height. The absorbed dose in the crystals gives the response to ionizing radiation except neutrons. The usage of GSI ball in combination with the GSI cylinder provides the possibility to measure the ambient equivalent dose from all particle types. In this work, sensitive TLD600H/700H chips [4] were used, which can provide reliable reading for dose from 2 μSv [16].

The passive detectors are used at GSI for long-time environmental monitoring and for pulsed radiation control, where active devices might show a pileup effect.

E. Gamma Detector

Two photon detectors have been tested in this work. Both of them are widely used for gamma ray dosimetry. The measured radiation quantity is ambient dose equivalent $H^*(10)$ and ambient dose rate equivalent $\dot{H}^*(10)$. One of these detectors is Berthold LB 1236-H10 [5], and it was used inside and outside the cave. The second detector is FHZ 621 G-L4-10

TABLE II
TECHNICAL DATA OF THE BERTHOLD LB 1236-H10 AND THERMO FISHER FHZ 621 G-L4-10

Detector	LB 1236-H10	FHZ 621 G-L4-10
Dose rate range	30 nSv/h → 20 mSv/h	100 nSv/h → 100 mSv/h
Energy range	35 keV → 1.3 MeV	30 keV → 1.3 MeV
Outer diameter	53 mm	65 mm
Length	550 mm	340 mm
Counter gas	Ar/CH4	Ar/CO2

from Thermo Fisher [4], and it was tested outside the Cave. The detectors contain a proportional counter tube and have a cylindrical shape. Table II presents some technical data on the photon probes and their dimensions.

III. READOUT ELECTRONICS

The radiation sensors convert the incident ionizing radiation into an electrical quantity such as current or voltage that could be readout by specific front-end electronics. Except for the ionization chambers, the other detectors used in this campaign use dedicated commercially available readouts. Though some commercial off-the-shelf solutions exist for ionization chambers, CERN developed a customized front-end because none of the solutions available on the market met the required specifications in terms of dynamic range, sensitivity, resolution, and bandwidth. This section presents the CERN custom developed CROME and ACCURATE front-ends for ionization chambers and the commercial readout systems used.

A. CROME Front-End

CROME is a state-of-the-art radiation monitoring system developed by CERN [11]. It is one of the main radiation monitoring systems used at CERN for the protection of personnel and is set to become the main system over the next few years. The front-end architecture of the system is shown in Fig. 1. For current measurement, the system exploits both slope tracking and current-to-frequency conversion (CFC) with reset counting methods [17]. The input current is integrated and fed through a driver to an analog-to-digital converter (ADC). The initial voltage at the start of the integration cycle and the final voltage at which the reset is applied are measured by the ADC. The problem of overshoot associated with the reset counting method is tackled by the ADC measurement. Three comparators with progressively higher thresholds generate outputs which are handled by the digital section. A reset pulse of predefined duration is generated depending on the comparator outputs.

B. Accurate ASIC Front-End

The current measurement front-end section of CROME relies on several critical components with almost no alternatives available on the market. To avoid the issues of obsolescence and to limit the number of discrete electronic components, the future version of the CERN radiation monitors will be based on an ASIC designed by the radiation protection team at CERN.

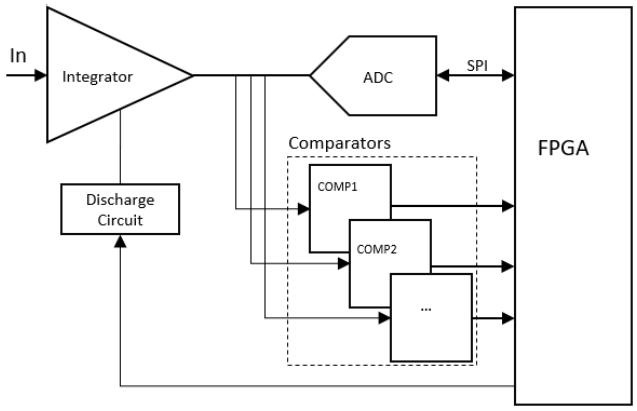

Fig. 1. CROME front-end system.

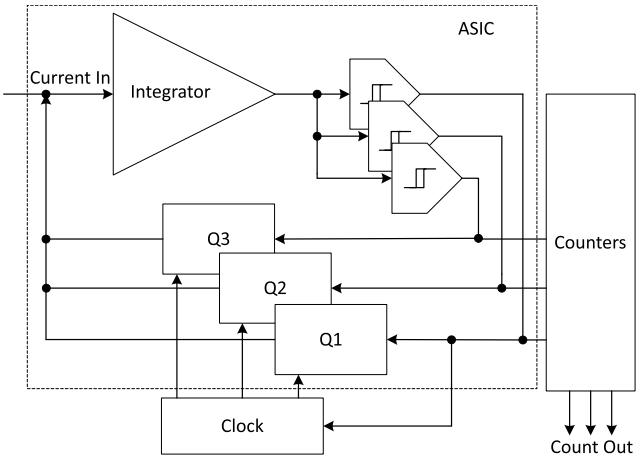

Fig. 2. ACCURATE front-end system.

The ASIC named ACCURATE could be interfaced directly with an ionization chamber to measure the current generated by the chamber. The architecture of the ASIC is shown in Fig. 2.

The ASIC works on the principle of charge-balancing CFC. The input current is integrated by an operational transconductance amplifier (OTA). The integrator output progressively enables three different comparators depending on the input current. The comparator outputs subsequently result in enabling charge generation sequentially thus injecting either $Q1$ or $Q1 + Q2$ or $Q1 + Q2 + Q3$ into the input node. This charge injection discharges the integrator and the process repeats. Counting the charge injections helps in calculating the input current. The ASIC output could thus be quantified as charges or the average current in a predefined time interval. In-depth details of the ASIC could be found in [18]. In the current experiment, both the charge output and current converted into dose rate are used in comparisons.

C. Area Monitor Display and Alarms FHT 1100 and FHT 6020

The gamma and neutron probes were connected to the Thermo Fisher's [4] electronics: FHT1100 and more recent version FHT6020. These devices are equipped with a flash EEPROM allowing communication with up to 16 different active dosimeters for the latest version (only two for the

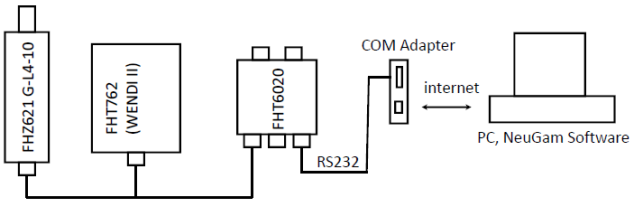

Fig. 3. FHT connection scheme.

earlier version) and providing local data storage if the personal computer (PC) connection to the devices is not established. During the experiment, the FHTs were connected to the internet via RS232 interface over W and T's [19] serial to TCP/IP communication adapter. The data were collected and stored on a PC using NeuGam Software, which allows for communication with multiple stations. The schematic layout of the connection can be seen in Fig. 3, which was used on top of Cave A with FHT6020 connected to FHT762 (WENDI-II) and FHZ621 G-L4-10 gamma probes. Inside Cave A, older version—FHT1100 in combination with FHT762 and Berthold's LB1236-H10 was used.

D. Readout System for TLDs

The TLD cards are readout in an automatic TLD reader (Harshaw TLD 6600 Plus). The system consists of two major components: the TLD reader and the Windows Radiation Evaluation and Management System (WinREMS) software residing on a PC, which is connected to the reader via an RS-232C serial communication port. The reader combines a medium capacity (200 TLD cards) transport system with a noncontact heating system for accurate and reproducible measurements. The Model 6600 Plus incorporates two parallel heating/data acquisition positions, enabling it to read two TL elements in one card simultaneously. The TLD cards and the TLD readers are now distributed by Thermo Fisher [4].

IV. Calibration of Detectors

The major constituent of the generated secondary radiation in the experimental setup was neutrons. Hence, it was necessary to calibrate the response of the used detectors to neutrons. Before the actual experiment, the pressurized and air-filled ionization chambers used were tested in the calibration laboratory at CERN with ^{241}Am-Be(α, n) source to determine their respective conversion factors.

For the calibration, the chambers were placed on a movable table which allows to vary the distance between the radiation source and the chamber. An 888 GBq source was used to vary the delivered dose rate from 50 to 1400 μSv/h. The PMI chambers were tested in the upper range starting from 100 μSv/h. For IG5 chambers, they were exposed in the lower range till 100 μSv/h. The current measured during each exposure was recorded using CROME. A conversion factor was thus derived for each dose rate. The measured conversion factor for different dose rates and the deviation of each step with the calculated average conversion factor for the PMI chambers are shown in Fig. 4.

For one PMI, the average conversion factor obtained is $(2.41 \pm 0.01) \times 10^{-9}$ A/Sv/h and that calculated for the second one is $(2.50 \pm 0.03) \times 10^{-9}$ A/Sv/h. Similarly derived

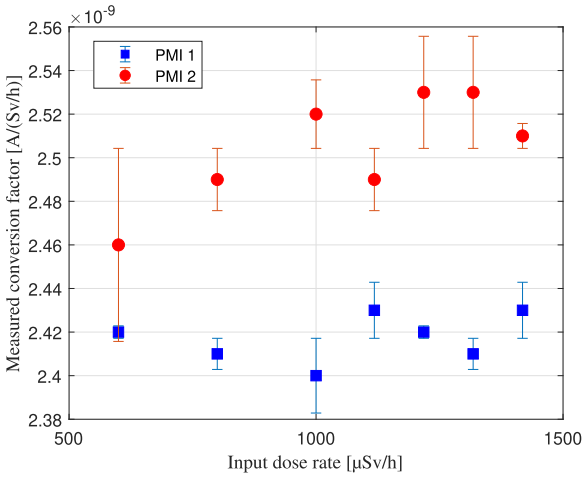

Fig. 4. Results of calibration of PMI chambers with AmBe sources.

conversion factors for IG5 are $(3.34 \pm 0.10) \times 10^{-8}$ A/Sv/h for IG5 1 and $(3.91 \pm 0.23) \times 10^{-8}$ A/Sv/h for IG5 2.

All the TLD 600H/700H cards used during the experiment have been calibrated with ^{137}Cs gamma radiation source with a nominal activity of 364 MBq. After determining the responses of every single crystal to gamma radiation, all the GSI balls used during experiments were calibrated in terms of neutron ambient dose equivalent using the neutron fields generated from ^{241}Am-Be(α, n) source with a nominal activity of 370 GBq. The calibration factor on average was 1.10 $\pm$ 0.05 μSv/μGy. To exclude any uncertainties coming from the dosimeter setup, the calibration was performed with exactly the same combination of cards and moderators used during the experiment. A detailed description of the neutron calibration procedure can be found in [1]. The GSI cylinders containing only TLD700H crystals in the cards were calibrated with ^{137}Cs source. Calibration factors to gamma radiation, obtained for TL crystals (four for each card) were: on average 0.59 $\pm$ 0.05 nC/μSv for TLD600H and 0.57 $\pm$ 0.04 nC/μSv for TLD700H.

WENDI-II and the two gamma detectors have nominal conversion factors from the manufacturer. In addition, the response to ^{241}Am-Be(α, n) and ^{137}Cs for WENDI-II and gamma probes, respectively, has been derived and the differences are about 20% for WENDI-II and gamma probes less than 10% to the nominal conversion factors.

V. Measurement Setup

The schematics of Cave A with relative positions of some of the detectors is shown in Fig. 5. The dosimeters were irradiated in the secondary radiation field generated by a 1-GeV/u ^{56}Fe beam fully stopped in a cylindrical polyethylene target 50 cm in diameter with a height of 25 cm. The angular position of the detectors within the cave is shown in Fig. 6. The primary beam was monitored during the irradiation with a parallel plate ionization chamber [20].

For the whole campaign, two positions were used inside the cave and one position outside on top of the cave. The position at an angle of around 27° in the corner of the cave is designated as location 1 and one at around 15° closer to the target as location 2. The ambient dose equivalents were measured with the GSI passive detector sets including

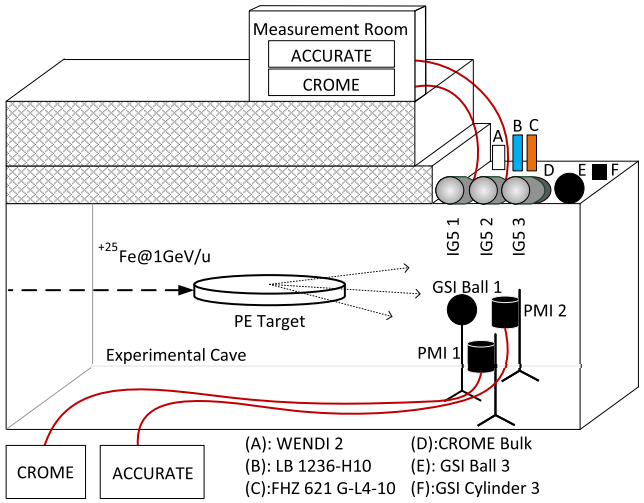

Fig. 5. Measurement setup.

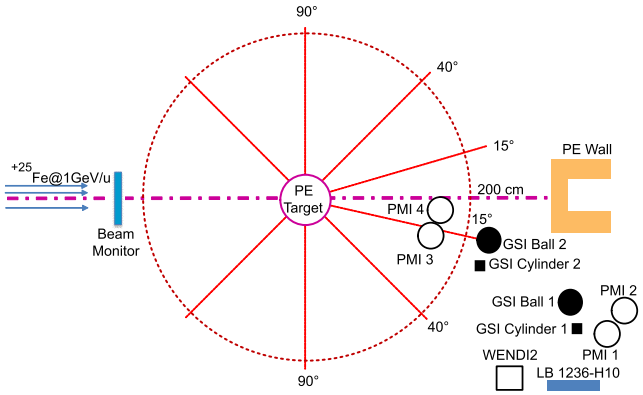

Fig. 6. Location of detectors in the measurement cave.

ball and cylinder at location 1 along with a WENDI-II and photon probe LB 1236-H10. Since for the high dose areas, air-filled ionization chambers are preferred over the pressurized chambers, PMI chambers were used for the measurements within the cave. Since the readout electronics are not designed to be radiation hard, the chambers were interfaced to their respective electronics using custom-made SPA6 cables. The supply of the high voltage for the chamber and transporting the charges generated from the chambers to the measurement electronics was handled using the same cable. PMI chamber 1 was interfaced to CROME and PMI 2 to the ACCURATE-based front-end. The same PMI chambers were moved closer to location 2 with the new designation PMI 3 at an angle of around 10° interfaced to CROME and PMI 4 at an angle of around 15° interfaced to ACCURATE. The same GSI ball and cylinder used at location 1 were also moved to location 2 with a new set of cards and are designated as GSI ball 2 and GSI cylinder 2 in Fig. 5.

For the roof of the cave, the detectors installed remained unchanged for the whole measurement. A WENDI-II with two different photon probes LB 1236-H10 and FHZ 621 G-L4-10 and one set of GSI passive detectors were located on the roof of Cave A (location 3). In addition, measurements were also carried out using three pressurized ionization chambers—IG5 1, IG5 2, and IG5 3. A CROME unit was used as the measurement electronics for IG5 1 and ACCURATE for IG5 2. IG5 3 used a configuration called CROME bulk in which the measurement electronics were attached to the chamber directly eliminating the need for cables.

VI. FLUKA Simulations

Using Flair [21], all the GSI Cave A relevant features, including shielding and experimental setup, were accurately reproduced for calculations. In this regard, Tables III and IV, respectively, summarize the densities used for the most relevant items included in the FLUKA geometry and the concrete shielding elemental composition. Since impurities were unknown, polyethylene target and dumps, as well as Cave A iron dump and other secondary structures were treated as pure materials. Considering the purpose of this study,

TABLE III

Densities of Polyethylene Target, Concrete Shielding, and Iron Structures Used in the Simulations

Component	Density ($g\,cm^{-3}$)
Polyethylene target	0.94
Concrete shielding	2.35
Iron structures	7.874

TABLE IV

Elemental Composition of Concrete Assumed in the Simulation (Given in Percent by Weight)

Element	Weight fraction (%)	Element	Weight fraction (%)
H	0.60	Al	2.0
C	0.40	Si	35.8
O	51.1	Ca	8.6
Na	0.3	Fe	1.2

possible traces in material compositions were assumed to have a negligible impact on the simulation outcome.

The detector regions were defined as air volumes having the same dimensions as the IG5, PMI, and GSI passive and active detectors used in the experiment; their positioning reflected their actual locations in the experimental setup.

As source term, a rectangular-shaped (5 cm in size in both the dimensions) beam of ^{56}Fe nuclei with a kinetic energy of 1 GeV/u was set up.

In the simulation, all the particles were transported until captured or ranged out. This allowed the full description of hadron and electromagnetic cascades. For hadrons, the transport threshold was set to 100 keV, except only for neutrons, which were followed down to thermal energies (transport threshold at 1×10^{-14} GeV) using FLUKA pointwise treatment for neutron transport [22]. Electrons, positrons, and photons were transported activating FLUKA electromagnetic transport option. For the first two species, the transport threshold was set to 100 keV, while the threshold was set to 1 keV for the latter. Being the beam particle ions, the full transport of all the light and heavy ions (including nuclear interactions) was enabled by default. A region-based importance biasing (particle-splitting algorithm) was put in place and applied to all the particles transported through Cave A concrete shielding.

Several quantities were assessed. For two detectors, namely, PMI in location 2 (inside the cave) and IG5 in location 3 (outside the cave), particle spectra were computed by scoring

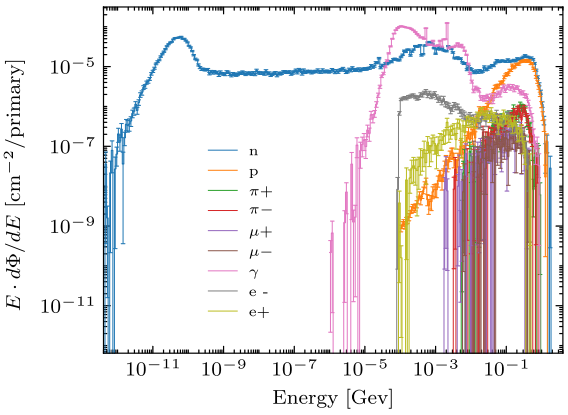

Fig. 7. Simulated fluence per lethargy unit for various particles inside a PMI detector (location 2, inside the experimental cave).

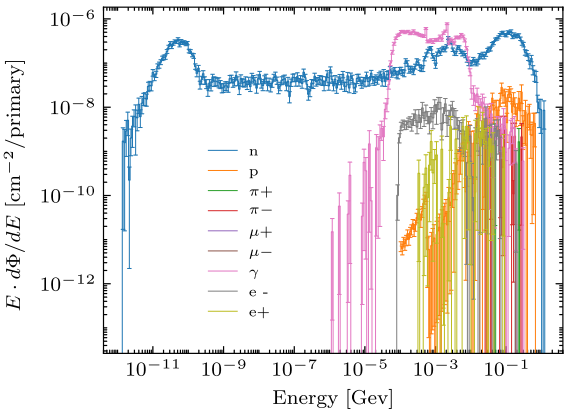

Fig. 8. Simulated fluence per lethargy unit for various particles inside an IG5 detector (location 3, outside the experimental cave).

the track length of all the particles reaching the two detector volumes (Figs. 7 and 8, respectively).

The ambient dose equivalent, $H^*(10)$, was evaluated inside the detector's volumes with region-based scorings and on a Cartesian mesh covering part of the cave. Fig. 9 shows a vertical cut of the $H^*(10)$ distribution (expressed in μSv per primary ion on target) inside and around GSI Cave A. Visible are the beam pipe ($z = 0$ to 1000 cm, $y = 200$ cm), the target ($z = 1000$ cm, $y = 200$ cm), some structures present inside the cave (dumps, detector supports), and concrete shielding. Outside of it, downstream with respect to the beam pipe, some detectors are represented.

Finally, the PMI and IG5 responses were simulated in FLUKA. For all the instruments (three IG5 and four PMI), all the particle track-fluences inside the detector volumes were estimated with a region-based scoring. A user routine, providing the energy-dependent factors (units: pC cm^2) [23], [24] for converting fluence inside the detector to charge collected in it by the detection system itself, was used to weight the fluences of the various particles at scoring time, yielding the detector response (charge per primary ion, Table V).

VII. Simulation Versus Measurement

Table V represents the comparison between the measured and simulated charges collected by both types of CERN detectors PMI and IG5 normalized per primary particles.

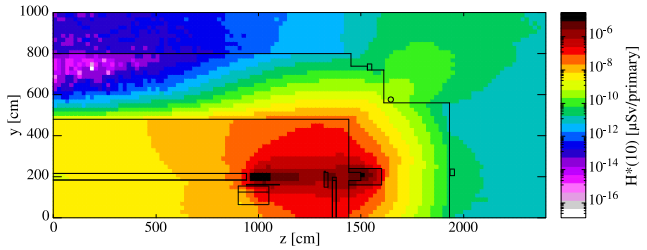

Fig. 9. Ambient dose equivalent map of GSI Cave A (vertical cut, crossing the beam pipe and the target), simulated with FLUKA v4-3.2.

TABLE V
Comparison of Measured Detector Response to Simulation for PMI and IG5 Detectors at Several Locations

Det.	Simulation [C/primary]	Measurement [C/primary]	Ratio (Sim. vs. Meas.)
PMI1	2.76E-18 ± 1.20%	2.99E-18 ± 5.08%	0.92 ± 5.22%
PMI2	3.28E-18 ± 1.03%	3.22E-18 ± 5.00%	1.02 ± 5.11%
PMI3	7.14E-17 ± 0.21%	5.54E-17 ± 5.06%	1.29 ± 5.06%
PMI4	3.93E-17 ± 0.25%	3.45E-17 ± 8.46%	1.14 ± 8.47%
IG5- 1	9.52E-20 ± 2.09%	1.18E-19 ± 5.00%	0.81 ± 5.42%
IG5- 2	7.55E-20 ± 2.45%	9.59E-20 ± 5.13%	0.79 ± 5.68%
IG5- 3	5.97E-20 ± 2.44%	7.73E-20 ± 5.22%	0.77 ± 5.76%

The contribution to the measurement uncertainty originates mainly from the uncertainty of the beam monitor calibration (about 5% [20]) and the standard deviation of the measured values from all runs. In addition, the inaccuracy of the detector position alignment was taken into account. The uncertainties of simulations presented in the table include only statistical errors. The comparisons between the simulated and measured results show an excellent agreement for all the detector positions.

The results for the ambient dose equivalent measured by the passive and active detectors at the different positions normalized per primary particles are reported in Table VI. At small angles, close to the incident beam direction, projectile fragments, mostly protons, with high energy, are able to produce a significant amount of neutrons inside the GSI ball itself, which also contribute to the measured neutron dose. So the measured neutron ambient dose equivalent should be corrected to the protons' contribution, which was done for the GSI balls at positions 1 and 2. A detailed description of proton corrections is presented in [1]. For the values measured with IG5 detectors from Table V, the conversion factors were applied to get the ambient dose equivalents. The results are also presented in Table VI. The determination of the conversion factors for IG5 was described in Section IV. The experimental results have been compared with FLUKA predictions of the ambient dose equivalent at all the measuring positions of the dosimeters. The neutron ambient dose equivalents were calculated for neutron dosimeters such as GSI balls and WENDI-II. For other detectors insensitive to neutrons (GSI Cylinders, LB 1236-H10 from Berthold and FHZ 621 G-L4-10 from Thermo Fisher), the corresponding FLUKA scorings were implemented to reflect the same behavior of the instrumentation. To do so, USRBIN scorings were coupled to a user-written fluscw.f routine that allowed to discard neutron contributions to ambient dose equivalent

TABLE VI
COMPARISON OF MEASURED AMBIENT DOSE EQUIVALENT TO SIMULATION FOR THE DETECTORS AT SEVERAL LOCATIONS

Location	Detector	Type of Radiation	Simulation H*(10) [μSv/primary]	Measurement H*(10) [μSv/primary]	Ratio (Sim. vs. Meas.)
1 inside	GSI ball 1	Neutrons	5.73E-08 ± 0.29%	4.82E-08 ± 9.51%	1.19 ± 9.51%
	GSI Cylinder 1	All particles without neutrons	2.52E-08 ± 4.16%	1.86E-08 ± 6.85%	1.36 ± 8.02%
	WENDI-II	Neutrons	4.32E-08 ± 0.44%	6.37E-08 ± 5.11%	0.68 ± 5.12%
	LB 1236-H10	All particles without neutrons	1.82E-08 ± 2.38%	1.24E-08 ± 7.14%	1.47 ± 7.53%
2 inside	GSI ball 2	Neutrons	1.54E-07 ± 0.18%	1.45E-07 ± 10.58%	1.06 ± 10.58%
	GSI Cylinder 2	All particles without neutrons	1.60E-07 ± 1.59%	1.73E-07 ± 5.89%	0.92 ± 6.10%
3 outside	IG5- 1	All particles	7.23E-10 ± 1.40%	8.52E-10 ± 5.00%	0.85 ± 5.19%
	IG5- 2	All particles	5.74E-10 ± 1.49%	6.81E-10 ± 5.13%	0.84 ± 5.34%
	IG5- 3	All particles	4.52E-10 ± 1.59%	5.02E-10 ± 5.22%	0.90 ± 5.45%
	GSI ball 3	Neutrons	5.06E-10 ± 1.19%	4.51E-10 ± 9.51%	1.12 ± 9.58%
	GSI Cylinder 3	All particles without neutrons	9.01E-11 ± 27.70%	1.12E-10 ± 6.35%	0.80 ± 28.42%
	WENDI-II	Neutrons	7.77E-10 ± 1.39%	9.86E-10 ± 5.19%	0.79 ± 5.38%
	LB 1236-H10	All particles without neutrons	5.60E-11 ± 13.16%	6.90E-11 ± 5.11%	0.81 ± 14.12%
	FHZ 621 G-L4-10	All particles without neutrons	8.25E-11 ± 13.72%	8.87E-11 ± 7.19%	0.93 ± 15.49%

directly at simulation time. The IG5 dosimeters can measure $H^*(10)$ from all types of ionizing radiation, and therefore, the ambient dose equivalent for all the particles at the positions of the IG5 detectors was calculated and is presented in Table VI. The ratios between the calculated and measured results show very good agreement, especially for the GSI passive dosimeters and IG5. The GSI balls have a deviation of less than 20% and the GSI cylinder is around 30%. The measured $H^*(10)$ values for all the active devices located on the roof of Cave A in comparison to the simulated ambient dose equivalents are less than 15% for IG5 dosimeters and are less than 30% for WENDI-II, LB 1236-H10, and FHZ 621 G-L4-10 detectors. The ambient dose equivalent measured with active detector WENDI-II inside the cave has a 30% deviation from the FLUKA simulation and the ambient dose equivalent measured with LB 1236-H10 from Berthold has a deviation of around 50%. These significant differences could be due to larger uncertainties in cave geometry in simulations.

VIII. MEASUREMENT RESULTS OF DIFFERENT DETECTORS

The ambient dose equivalent rate measurement by CROME within the cave and on the roof is depicted in Fig. 10. As expected, the dose rate measured by the PMI chambers within the cave with the mixed field is significantly higher than that measured by IG5 on the roof which is dominated by neutrons.

To compare the response between all the detectors used, the result from the first run alone is plotted in Fig. 11. The ambient dose equivalent rates measured by different detectors during the first run are calculated using the calibration factors obtained by the method explained in Section IV. Since the conversion factors used were derived with different setups, a direct comparison of the ambient dose equivalent rate measured is not meaningful, but it is interesting to observe that the time structure of the dose rate measurement remains constant across the detectors. CROME and ACCURATE front-ends, which are both connected to PMI chambers in the cave and hence have comparable conversion factors, reported similar data rates.

The WENDI-II and gamma probes' detectors reported an output every 10 s. The CROME and ACCURATE front-end measures with a time resolution of 100 ms. Hence for these two measurements, a moving average with a width of 100 points was used to generate comparable results across detectors. From the recorded measurements of CROME and ACCURATE devices, the temporal response of the generated pulses could be observed. It could be seen that each spill width is around 10 s and is perfectly discernible as shown in Fig. 12.

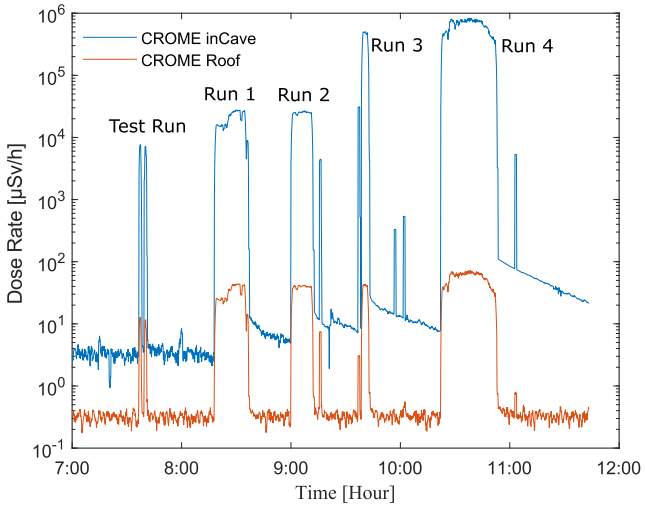

Fig. 10. Ambient dose equivalent rates measured by CROME detectors for the entire measurement campaign.

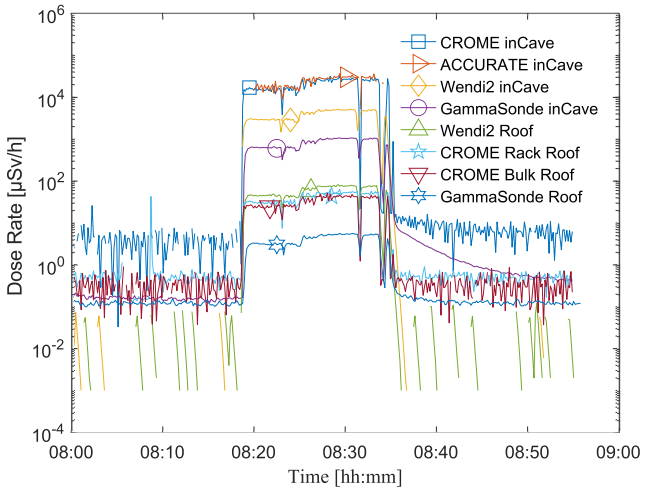

Fig. 11. Ambient dose equivalent rates measured by different detectors during the first run.

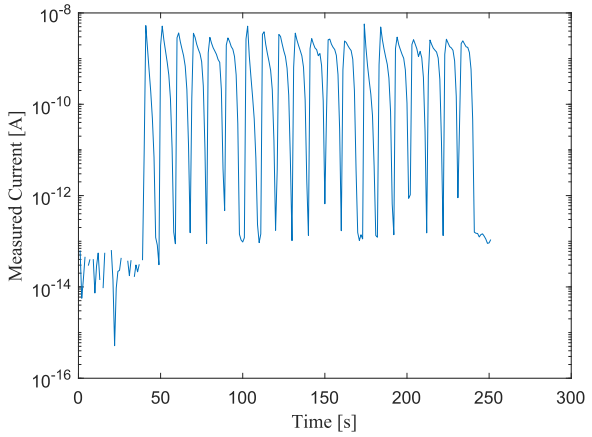

Fig. 12. Current measured by CROME detector in the cave for Run 3.

The wide dynamic range spanning from around 1 fA to 5 nA as observed in this run and recorded by CROME could also be seen in Fig. 12.

IX. Conclusion

This article described a very complex measurement campaign carried out at a heavy ion accelerator facility. The main goal of this first-of-its-kind campaign was the comparison of different kinds of radiation monitors in a radiation field dominated by neutrons and light ions. The various detectors used reported very comparable time responses throughout the campaign. In addition, FLUKA Monte Carlo radiation transport simulations were performed to obtain the spectral particle fluences and the ambient dose equivalent as well as the detector responses for different exposure positions inside and outside Cave A. The agreement between the measured and simulated responses of the tested detectors is better than a factor of 1.4, demonstrating that FLUKA is a well-suited tool when predicting the responses of dosimeters. Finally, the charges measured by the existing front-end of the CERN radiation monitor (CROME) and that measured by the future front-end (ACCURATE) were comparable with a relative mismatch in accordance with the position of the respective ionization chambers. It was also worth noting that the active CERN radiation monitors had a measurement resolution of 100 ms which aided in precisely understanding the time structure of the recorded pulses. Such capabilities could be useful in potential future applications where the radiation environment would be predominately pulsed and accurate measurement of charges per pulse is a requirement. The promising performance demonstrated by ionization-chamber-based radiation monitors also paves the path to evaluating them further for potential use in future facilities like FAIR [25].

Acknowledgment

The authors would like to thank Kolja Beverung for creating remote control system software NeuGam and for valuable advice and discussions during the experiment.

References

[1] D. Boscolo et al., "Characterization of the secondary neutron field produced in a thick aluminum shield by 1 GeV/u ^{56}Fe ions using TLD-based ambient dosimeters," *Frontiers Phys.*, vol. 8, p. 365, Feb. 2020.

[2] A. Sokolov et al., "Neutron spectra at a high energy heavy ion accelerator measured with a TLD-based bonner spectrometer," *J. Instrum.*, vol. 16, no. 10, Oct. 2021, Art. no. P10022. [Online]. Available: https://iopscience.iop.org/article/10.1088/1748-0221/16/10/P10022/meta

[3] F. Horst et al., "A multi-detector experimental setup for the study of space radiation shielding materials: Measurement of secondary radiation behind thick shielding and assessment of its radiobiological effect," in *Proc. EPJ Web Conf.*, vol. 261, 2022, Art. no. 03002, doi: 10.1051/epjconf/202226103002.

[4] *Thermo Fisher*. [Online]. Available: https://www.thermofisher.com

[5] *Berthold*. [Online]. Available: https://www.berthold.com

[6] J. Farah et al., "Measurement of stray radiation within a scanning proton therapy facility: EURADOS WG9 intercomparison exercise of active dosimetry systems," *Med. Phys.*, vol. 42, no. 5, pp. 2572–2584, May 2015.

[7] S. Mayer et al., "Response of neutron detectors to high-energy mixed radiation fields," *Radiat. Protection Dosimetry*, vol. 125, nos. 1–4, pp. 289–292, Dec. 2006.

[8] C. Ahdida et al., "New capabilities of the FLUKA multi-purpose code," *Frontiers Phys.*, vol. 9, Jan. 2022, Art. no. 788253.

[9] G. Battistoni et al., "Overview of the FLUKA code," *Ann. Nucl. Energy*, vol. 82, pp. 10–18, Aug. 2015.

[10] *FLUKA*. [Online]. Available: https://fluka.cern

[11] H. Boukabache et al., "Towards a novel modular architecture for CERN radiation monitoring," *Radiat. Protection Dosimetry*, vol. 173, nos. 1–3, pp. 240–244, 2017.

[12] S. K. Mohanan, H. Boukabache, V. Cruchet, D. Perrin, S. Roesler, and U. R. Pfeiffer, "An ultra low current measurement mixed-signal ASIC for radiation monitoring using ionisation chambers," *IEEE Sensors J.*, vol. 22, no. 3, pp. 2142–2150, Feb. 2022.

[13] *International Commission on Radiation Units and Measurements (ICRU)*, Oper. Quantities External Radiat. Exposure, Int. Commission Radiat. Units Meas., Inc. (ICRU), Bethesda, MD, USA, 2020.

[14] F. Gutermuth, T. Radon, G. Fehrenbacher, and J. G. Festag, "The response of various neutron dose meters considering the application at a high energy particle accelerator," *Kerntechnik*, vol. 68, no. 4, pp. 172–179, Mar. 2022.

[15] G. Fehrenbacher, F. Gutermuth, E. Kozlova, T. Radon, and R. Schuetz, "Neutron dose measurements with the GSI ball at high-energy accelerators," *Radiat Prot Dosimetry*, vol. 125, pp. 209–212, Jul. 2007.

[16] E. Kozlova, A. Sokolov, M. Pyshkina, and T. Radon, "Testing of new sensitive TLD cards," *GSI Sci. Rep.*, vol. 1, p. 375, Sep. 2017.

[17] S. K. Mohanan, H. Boukabache, D. Perrin, and U. R. Pfeiffer, "Comparative analysis of ultra-low current measurement topologies with implementation in 130 nm technology," *IEEE Access*, vol. 9, pp. 63855–63864, 2021.

[18] S. Kundumattathil Mohanan, "An accurate ultra-low current measurement ASIC for ionization chamber readout," Ph.D. dissertation, Dept. Radiat. Protection, CERN, 2021.

[19] *WuT*. [Online]. Available: https://www.wut.de

[20] F. Luoni et al., "Beam monitor calibration for radiobiological experiments with scanned high energy heavy ion beams at FAIR," *Frontiers Phys.*, vol. 8, Sep. 2020, Art. no. 568145. [Online]. Available: https://www.frontiersin.org/articles/10.3389/fphy.2020.568145

[21] V. Vlachoudis, "FLAIR: A powerful but user friendly graphical interface for FLUKA," in *Proc. Int. Conf. Math., Comput. Methods React. Phys.*, New York, NY, USA, 2009, pp. 1–11.

[22] V. Vlachoudis et al., "Recent developments in the point wise neutron treatment for FLUKA v4," in *Proc. EPJ Web Conf.*, vol. 284, 2023, Art. no. 03021, doi: 10.1051/epjconf/202328403021.

[23] H. Vincke, D. Forkel-Wirth, D. Perrin, and C. Theis, "Simulation and measurements of the response of an air ionisation chamber exposed to a mixed high-energy radiation field," *Radiat. Protection Dosimetry*, vol. 116, nos. 1–4, pp. 380–386, Dec. 2005, doi: 10.1093/rpd/nci088.

[24] C. Theis, D. Forkel-Wirth, D. Perrin, S. Roesler, and H. Vincke, "Characterisation of ionisation chambers for a mixed radiation field and investigation of their suitability as radiation monitors for the LHC," *Radiat. Protection Dosimetry*, vol. 116, nos. 1–4, pp. 170–174, Dec. 2005, doi: 10.1093/rpd/nci097.

[25] J. Blaurock, H. Simon, P. Spiller, and O. Boine-Frankenheim, "FAIR completion of construction works, towards commissioning and first science," in *Proc. IPAC*, 2023, pp. 3923–3927.